A Shared Binding Site for NAD^+ and Coenzyme A in an Acetaldehyde Dehydrogenase Involved in Bacterial Degradation of Aromatic Compounds[†]

Yu Lei, Peter D. Pawelek, and Justin Powlowski*

Department of Chemistry and Biochemistry, Concordia University, 7141 Sherbrooke Street West, Montreal, Quebec, Canada H4B 1R6

Received February 29, 2008; Revised Manuscript Received May 10, 2008

ABSTRACT: The *meta*-cleavage pathway for catechol is a central pathway for the bacterial dissimilation of a wide variety of aromatic compounds, including phenols, methylphenols, naphthalenes, and biphenyls. The last enzyme of the pathway is a bifunctional aldolase/dehydrogenase that converts 4-hydroxy-2-ketovalerate to pyruvate and acetyl-CoA via acetaldehyde. The structure of the NAD^+/CoASH-dependent aldehyde dehydrogenase subunit is similar to that of glyceraldehyde-3-phosphate dehydrogenase, with a Rossmann fold-based NAD^+ binding site observed in the NAD^+−enzyme complex [Manjasetty, B. A., et al. (2003) *Proc. Natl. Acad. Sci. U.S.A. 100*, 6992−6997]. However, the location of the CoASH binding site was not determined. In this study, hydrogen−deuterium exchange experiments, coupled with peptic digest and mass spectrometry, were used to examine cofactor binding. The pattern of hydrogen−deuterium exchange in the presence of CoASH was almost identical to that observed with NAD^+, consistent with the two cofactors sharing a binding site. This is further supported by the observations that either CoASH or NAD^+ is able to elute the enzyme from an NAD^+ affinity column and that preincubation of the enzyme with NAD^+ protects against inactivation by CoASH. Consistent with these data, models of the CoASH complex generated using AUTODOCK showed that the docked conformation of CoASH can fully occupy the cavity containing the enzyme active site, superimposing with the NAD^+ cofactor observed in the X-ray crystal structure. Although CoASH binding Rossmann folds have been described previously, this is the first reported example of a Rossmann fold that can alternately bind CoASH or NAD^+ cofactors required for enzymatic catalysis.

Aldehyde dehydrogenases make up a diverse group of enzymes that are present in a wide variety of organisms, including mammals, plants, bacteria, and fungi. These enzymes may be categorized on the basis of cofactor dependence: (i) $NAD(P)^+$-independent aldehyde dehydrogenases such as EC 1.2.99.3 and EC 1.2.7.5, which are found in some bacteria (*1, 2*); (ii) $NAD(P)^+$-dependent aldehyde dehydrogenases such as EC 1.2.1.3 and related enzymes, which have been isolated from both prokaryotes and eukaryotes (*3–5*); and (iii) CoASH/$NAD(P)^+$-dependent aldehyde dehydrogenases such as EC 1.2.1.10 and EC 1.2.1.27, which are mainly associated with a few species of bacteria (*6–15*). While $NAD(P)^+$-dependent members of the aldehyde dehydrogenase (ALDH) extended family have been well characterized (*3–5*), CoASH/$NAD(P)^+$-dependent aldehyde dehydrogenases have received much less attention.

The literature on CoASH/$NAD(P)^+$-dependent aldehyde dehydrogenases focuses mainly on the steady-state kinetics and some other properties of a few individual members (*6–10, 13–15*). For example, a relatively well-characterized coenzyme A-linked aldehyde dehydrogenase from *Clostridium kluyveri* (*10*) catalyzes the transformation of acetaldehyde to acetyl-CoA accompanied by NAD^+ reduction with a pH optimum of 9.1. On the basis of initial velocity and product inhibition experiments, a ping-pong mechanism was proposed. Thus, NAD^+ and acetaldehyde bind first, NADH is released prior to CoASH binding, and then the final product, acetyl-CoA, is released. Formation of an acetyl−enzyme intermediate during the reaction was postulated. Interestingly, inhibition by CoASH was also reported, and the formation of a dead-end E−CoASH inhibition complex was demonstrated (*10*).

DmpF (EC 1.2.1.10) is the only CoASH/$NAD(P)^+$-dependent aldehyde dehydrogenase for which a high-resolution structure has been published. DmpF and DmpG form an active heterotetramer (F_2G_2) which catalyzes the last two reactions in the *meta*-cleavage pathway of phenol degradation in *Pseudomonas* sp. strain CF600 (*16*). DmpG (EC 4.1.3.39) is a type II aldolase that converts 4-hydroxy-2-ketovalerate to acetaldehyde and pyruvate, while DmpF catalyzes the transformation of acetaldehyde to acetyl-CoA using NAD^+ and CoASH. The X-ray structure of DmpFG (*17*) shows eight polypeptide chains in the asymmetric unit: four DmpGs (A, C, E, and G) and four DmpFs (B, D, F, and H) that form two heterotetramers each with a molecular mass of 280 kDa. DmpF comprises two domains, including the NAD^+ binding domain (residues 1−130 and 286−312) and the dimerization domain (residues 131−285) which mediates the interaction with DmpG.

[†] This work was supported by a Discovery program grant to J.P. from the Natural Sciences and Engineering Research Council of Canada.

* To whom correspondence should be addressed. Telephone: (514) 848-2424, ext. 5664. Fax: (514) 848-2868. E-mail: powlow@alcor.concordia.ca.

10.1021/bi800349k CCC: $40.75
Published on Web 06/07/2008

```
          β1              α1              β2          α2          β3
  1  MNQKLKVAIIGSGNIGTDLMIKVLRNAKYLEMGAMVGIDAASDGLARAQRMGVTTTYAGV
       α3   α4   β4              α5              β5              α6
 61  EGLIKLPEFADIDFVFDATSASAHVQNEALLRQAKPGIRLIDLTPAAIGPYCVPVVNLEE
          β6        α7                  β7      α8   α9      α10
121  HLGKLNVNMVTCGGQATIPMVAAVSRVAKVHYAEIVASISSKSAGPGTRANIDEFTETTS
                  β8                  β9              α11
181  KAIEVIGGAAKGKAIIIMNPAEPPLIMRDTVYVLSAAADQAAVAASVAEMVQAVQAYVPG
     β10      β11      β12  β13    β14                         α12
241  YRLKQQVQFDVIPESAPLNIPGLGRFSGLKTSVFLEVEGAAHYLPAYAGNLDIMTSAALA

301  TAERMAQSMLNA
```

FIGURE 1: Secondary structural elements of DmpF. Residues shaded dark gray highlight β strands, while residues shaded light gray highlight α-helical regions (derived from PDB entry 1NVM).

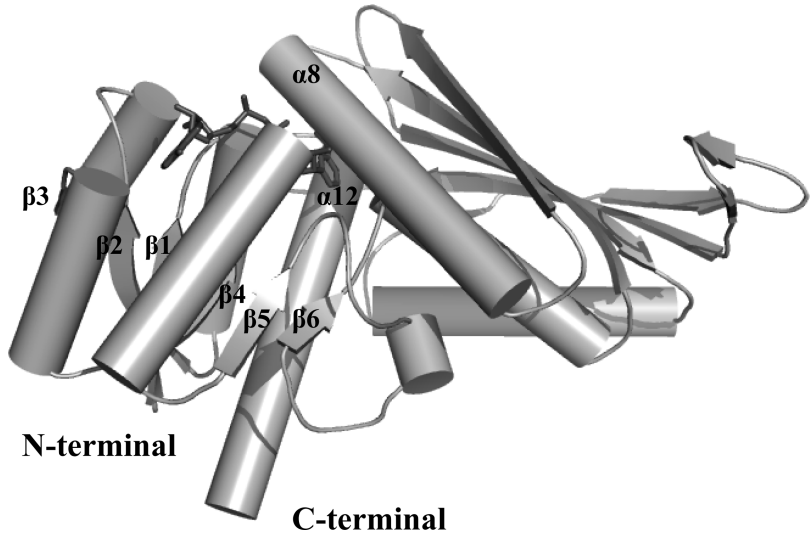

FIGURE 2: Structural overview of the NAD^+−DmpF complex. $\beta1-\beta6$ represent the six-stranded parallel sheet that comprises the typical Rossman fold mainly involved in AMP binding; α8 and α12 are mainly responsible for the NMN binding together with other structural elements (derived from PDB entry 1NVM).

The NAD^+-binding domain of DmpF is similar to that of glyceraldehyde-3-phosphate dehydrogenase (phosphorylating) (*17*). Sequence analysis using the Pfam database (*18*) shows that the NAD^+-binding domain belongs to the NADP_Rossmann clan and most closely resembles the family Semialdhyde_dh with an *E* value of 1.4×10^{-24}; the structure of aspartate semialdehyde dehydrogenase, also a phosphorylating enzyme, has an NAD^+ binding fold similar to that of glyceraldehyde-3-phosphate dehydrogenase (*19*). By contrast, another CoASH/$NAD(P)^+$-dependent enzyme, methylmalonate semialdehyde dehydrogenase (EC 1.2.1.27), is instead structurally related to the large superfamily of nonphosphorylating aldehyde dehydrogenases and is the only member which is CoASH-dependent (*5, 15, 20*). As discussed below, DmpF, like glyceraldehyde-3-phosphate dehydrogenase (phosphorylating), binds NAD^+ via a canonical Rossmann fold. By contrast, nonphosphorylating aldehyde dehydrogenases exhibit noncanonical Rossmann folds for NAD^+ binding (*20–23*). Thus, CoASH-dependent aldehyde dehydrogenases belonging to the two families may bind CoASH differently. However, no structure has yet been published for a member of either class in complex with CoASH.

Two glycine-rich motifs that are characteristic of nucleotide binding domains are found in DmpF: $G_{11}XGXXG_{16}$ located between the loop following the first β strand and the adjacent α helix of the Rossmann fold and G_{165}-$XGXXA_{170}$ in the loop adjacent to α8, in the α9 helix, and in its following loop, which are located in the dimerization domain (Figure 1). The NAD^+-binding Rossmann fold consists of one each of $(\beta\alpha)_3$ and $(\alpha\beta)_3$ units in which the $(\beta\alpha)_3$ unit (residues 5−65) is mainly involved in AMP moiety binding and the $(\alpha\beta)_3$ unit (residues 67−128) is mainly responsible for NMN moiety binding (Figure 2); these units are connected via the α3 and α4 helices. Like glyceraldehyde-3-phosphate dehydrogenase (phosphorylating) and aspartate semialdehyde dehydrogenase, the dimerization domain of DmpF is also involved in NAD^+ binding, mainly via the NMN moiety. The AMP portion of bound NAD^+ is closest to the outside environment, while the NMN portion is located in the interior of the protein and encompassed by both NAD^+ binding and dimerization domains.

The conformation of NAD^+ when bound to DmpF is very similar to the conformation observed in complex with glyceraldehyde-3-phosphate dehydrogenase from *Bacillus stearothermophilus* (PDB entry 1GD1) (*17, 24*). Thus, both the adenine and nicotinamide rings are in anti conformations and approximately perpendicular to the adjacent ribose rings. The two ribose ring planes are perpendicular to each other. The AMP portion is more elongated than the NMN portion, and both moieties are on the same side relative to the phosphates. The NMN moiety is in the proximity of the rest of the molecule, so it is only half the distance from the nicotinamide group to the closest phosphate as it is in bound NAD^+ on other enzymes such as horse liver alcohol dehydrogenase (PDB entry 2OHX) (*25*).

Although a structure of the NAD^+−DmpF complex has been obtained using X-ray crystallography, the mode of binding of coenzyme A has not been defined. In this study, we have used hydrogen−deuterium exchange experiments to probe the binding of CoASH and have found that this cofactor shares the same binding site as NAD^+.

EXPERIMENTAL PROCEDURES

Bacterial Strains and Plasmids of Escherichia coli. XL2-Blue was used for DNA and plasmid amplification, and proteins were expressed in *E. coli* C41(DE3) (*26*). DNA manipulations were performed using standard protocols (*27*). A subclone of pVI150, pVI1316Δ (*28*), was digested with *Xho*II to generate a 3757 bp fragment that was subsequently ligated into the *Bam*HI site of the pT7.5 expression vector (*29*). Orientation was checked by restriction enzyme digestion. The *dmpFG* coding region was thus inserted downstream from the T7 promoter, to give plasmid construct pT7.5-*dmpFG*.

Bacterial Growth. The pT7.5-*dmpFG* plasmid (10 ng) was transformed into *E. coli* C41(DE3) competent cells by incubating the mixture on ice for 15−20 min. Cells (50 μL) were then spread onto LB agar plates to grow overnight at 37 °C using carbenicillin selection (100 μg/mL). LB medium (10 mL) was added to each plate to suspend the colonies. After transfer of the suspended cells into 1 L of fresh LB medium containing ampicillin (100 μg/mL), cells were grown for 2 h until the OD_{600} reached 0.8−1, at which point IPTG (1 mM) was added to induce protein overexpression. Cells were allowed to grow for an additional 3 h before being harvested. After being washed with 50 mM Na^+K^+ phosphate buffer (pH 7.5), cell pellets were stored at −80 °C until they were used.

Preparation of Affinity Resin. N^6-Carboxymethyl-NAD^+ was synthesized essentially as described by Tynan et al. (*30*). An excess of N^6-carboxymethyl-NAD^+ was coupled at 4 °C to EAH-Sepharose (GE Healthcare) using 1-ethyl-3-[3-(dimethylamino)propyl]carbodiimide, essentially as described by the manufacturer except that pH was maintained between 4.5 and 5.5 by the addition of HCl, as described in ref *30*. After incubation overnight, the resin was washed thoroughly using several alternating aliquots of 0.1 M sodium acetate (pH 4), containing 0.5 M NaCl, and 0.1 M Tris-HCl (pH 8), containing 0.5 M NaCl. A final wash of 20% ethanol was applied.

Protein Purification. Compared to the previously published method (*16*), the steps for purifying DmpFG were simplified to DEAE and NAD^+-linked affinity columns, combined with an ammonium sulfate fractionation step. The buffer used for purification was 50 mM Na^+K^+ phosphate (pH 7.5) containing 1 mM DTT[1] (PD buffer) unless otherwise specified, and all the purification steps were carried out at 4 °C. Approximately 25 g of cell paste from 6 L of culture was resuspended in ∼50 mL of PD buffer, and a spatula tip of DNase I was added. Cell suspensions in a salt/ice bath were sonicated in 30 mL batches with a Branson model 250 sonifier at an output setting of 60 for 10 × 25 s. The cell debris was removed by ultracentrifugation for 1 h at 62000*g*. The clear supernatant, termed crude extract, was carefully transferred to a 100 mL cylinder and then applied to a Fast-Flow DEAE-Sepharose column (36.5 cm × 2.6 cm) equilibrated with PD buffer. After the sample had been loaded, the column was washed with PD buffer (100 mL) and then with PD buffer containing 50 mM NaCl (200 mL) at a flow rate of 6 mL/min. A linear gradient from 0.05 to 0.275 M NaCl in PD buffer (750 mL/750 mL) was applied at a rate of 6 mL/min. Fractions (12 mL) were collected, and those with high CoASH-dependent acetaldehyde dehydrogenase specific activity were combined. DmpFG was precipitated with 55% saturated ammonium sulfate and then kept in an ice bath for least 30 min before being collected by centrifugation. The protein precipitate was dissolved in PD buffer to a total volume of 5 mL. After being desalted with a PD-10 column, the protein was applied to an NAD^+ affinity column (3.3 cm × 1.7 cm). The column was washed with 25 mL of PD buffer and then eluted using 0.1 M NaCl in PD buffer. Fractions (2 mL) were collected, and those with high dehydrogenase specific activity were combined. The sample was exchanged with 50 mM Na^+K^+ phosphate (pH 7.5) containing 0.5 mM TCEP-HCl two to five times and then finally concentrated to ∼2 mL. This operation was performed by ultrafiltration using an Amicon concentrator equipped with a YM-30 membrane. The concentrated protein was aliquoted into microfuge tubes (20−50 μL/tube) and then stored at −80 °C. The activity was stable for at least 6 months (*16*).

Deuterium Exchange Experiments. Deuterium exchange experiments essentially followed previously published methods (*31–33*). The pH measurements were performed with an Orion Micro-Combination pH/Sodium Electrode 98-10. All pH values of D_2O-containing buffers reported here were corrected using the equation $pH = pD + 0.3139x + 0.0854x^2$ (*34*), where pD is the pH meter reading of the buffer and x is the fraction of deuterium. Three different samples were equilibrated at 25 °C for 1 h: (1) 22 μL of DmpFG protein [8.53 mg/mL, 121.8 μM, in 50 mM Na^+K^+ phosphate buffer (pH 7.5) containing 0.5 mM TCEP-HCl] with 5.5 μL of 50 mM Na^+K^+ phosphate buffer (pH 7.5) containing 0.5 mM TCEP-HCl; (2) 22 μL of DmpFG protein with 5.5 μL of 10.1 mM NAD^+ in 50 mM Na^+K^+ phosphate buffer (pH 7.5) containing 0.5 mM TCEP-HCl; and (3) 22 μL of DmpFG protein with 5.5 μL of 11.5 mM CoASH in 50 mM Na^+K^+ phosphate buffer (pH 7.5) containing 0.5 mM TCEP-HCl.

The H−D exchanges were initiated by transferring the equilibrated samples with multichannel pipettors to aliquots (192.5 μL) of 50 mM Na^+K^+ phosphate D_2O buffer (pH 7), 25 °C, without cofactors, with NAD^+ (2.05 mM), or with CoASH (2.3 mM). These reaction mixtures were contained in 250 μL thin-walled PCR tubes inserted in a metal heat block kept in a 25 °C water bath. The H−D exchange reactions were thus carried out at 25 °C, at pH 7.09, and with 87.5% D_2O buffer. At various time points, 20 μL of each of the three different samples was transferred to mixtures in PCR tubes containing 110 μL of 0.12% TFA and a pellet from 80 μL of immobilized pepsin slurry (on cross-linked 6% agarose beads, 2−3 mg/mL of gel, pur-

[1] Abbreviations: DTT, dithiothreitol; ESI, electrospray ionization; FCT, formyl-CoA transferase; H−D exchange, hydrogen−deuterium exchange; MALDI, matrix-assisted laser desorption ionization; PDB, Protein Data Bank; SCS, succinyl-CoA synthetase; SDS−PAGE, sodium dodecyl sulfate−polyacrylamide gel electrophoresis; TCEP, tris(2-carboxyethyl)phosphine hydrochloride; TFA, trifluoroacetic acid.

chased from Pierce Chemical Co.). Mixing with TFA resulted in a pH of 2.56, effectively quenching the exchange, with the PCR tubes kept at 0 °C by insertion in a metal block which was incubated in an ice/salt water bath. The immobilized pepsin had been prepared by being washed six times with 0.05% TFA (pH 2.41), and in separate experiments monitored using SDS−PAGE, it was established that the pellet from 80 μL of the immobilized pepsin slurry was sufficient to digest completely the DmpFG protein in these samples (data not shown). To facilitate digestion efficiency, up-and-down operation of a multiple-channel pipettor was used to mix the protein and the immobilized pepsin. After 5 min, the digested samples were separated from immobilized pepsin by centrifugation in a microfuge at top speed for 40 s; the supernatants were then aliquoted into thin-wall PCR tubes and frozen in liquid nitrogen. The frozen samples were stored at −80 °C prior to mass spectrometry analysis.

In- and Back-Exchange Controls for Deuterium Incorporation. The extent of deuterium incorporation into each peptic peptide must be adjusted for deuterium gain and loss during quench, peptic digestion, and mass spectrometric analysis. The amount of deuterium lost and gained from a partially deuterated peptide may be estimated from the amount of deuterium lost from a completely exchanged peptide ("back-exchange" or "100% control") and gained from a unexchanged peptide ("in-exchange" or "0% control"), respectively. The in- and back-exchange control experiments were carried out according to methods described previously (*33, 35*). The in-exchange control (0% control) was performed by addition of 2 μL of DmpFG protein to the 0 °C mixture of 110 μL of 0.12% TFA and a pellet from 80 μL of immobilized pepsin slurry, 0.5 μL of 50 mM Na^+K^+ phosphate H_2O buffer (pH 7.5), and 17.5 μL of 50 mM Na^+K^+ phosphate D_2O buffer (pH 7). The digestion and associated procedures were the same as those in the deuterium exchange experiments reported above. The back-exchange control (100% control) was started by dissolving the peptic digest of DmpFG dried from the unexchanged control sample (prepared as described below) in 2.5 μL of H_2O and 17.5 μL of D_2O, producing a mixture containing concentrations of peptides, buffer, and deuterium corresponding to those of the H−D exchange experiments. Samples were then incubated at 25 °C for 2 h to ensure 100% deuterium replacement of the amide hydrogens in the peptides derived from the intact protein. After addition of 110 μL of 0.12% TFA at 0 °C, samples were incubated at 0 °C for the same time period required for sample quenching to pepsin bead isolation, as in the deuterium exchange experiments.

Measurements of Protected Amide Hydrogens, Incorporated Deuterons, and Their Exchange Rate Constants for Peptic Digests of DmpFG. The matrix used in the MALDI experiments was α-cyano-4-hydroxycinnamic acid (5 mg/mL) in an acetonitrile/99% ethanol/0.07% TFA mixture (1:1:1) (pH 2.5). The matrix solution was kept at 0 °C before use. Frozen sample digests were thawed rapidly, and 10 μL was mixed with an equal volume of matrix; 0.7 μL of the mixture was spotted onto the chilled target plate. The sample spots were dried with a stream of nitrogen gas over 1 min. The spotted and dried target plate was transferred as quickly as possible to the mass spectrometer. The spectra were collected using a Micromass M@LDI-LR TOF mass spectrometer. Spectra were obtained for both deuterium-exchanged samples and unexchanged controls in which the sample was prepared under identical conditions except that buffer prepared with H_2O was substituted for D_2O-containing buffer: these samples were used for sequencing peptides using ESI-Q-TOF MS/MS (details below).

By comparing the spectra of exchanged samples with those of unexchanged controls, we identified the peptides with deuterium incorporation. When masses of peptides from H−D experiments with cofactors shifted at least 0.5 Da lower relative to those incubated without cofactors, peptides were considered to have undergone amide hydrogen protection by cofactor binding. The number of amide hydrogens protected was estimated by comparing mass differences of the H−D exchange peptides from incubations with and without cofactor. The number of deuterons incorporated into peptic digest peptides of DmpFG was calculated using the equation $D = (m_t - m_{0\%}) \times n/(m_{100\%} - m_{0\%})$, where D is the adjusted number of deuteriums incorporated at time t, m_t, $m_{0\%}$, and $m_{100\%}$ are the observed masses of a peptide at time t, time zero (0% control), and fully exchanged (100% control), respectively, and n is the total number of peptide amide hydrogens. The rate constants for deuterium exchange were obtained by fitting the data to a double-exponential model using SigmaPlot 9.0 with the equation $D = N_1(1 - e^{-k_1 t}) + N_2(1 - e^{-k_2 t})$, where D is the total number of incorporated deuterons at time t and N_1 and N_2 are the numbers of deuterons exchanging at rate constants k_1 and k_2, respectively. A mixture of six standards, bradykinin (1060.569 amu), angiotensin I (1296.687 amu), Substance-P (1347.736 amu), Glu-fibrino peptide (1570.677 amu), renin (1758.933 amu), and ACTH (18-39clip, 2465.199 amu), was used to calibrate the instrument. Internal lockmass corrections using ACTH (18-39clip, 2465.199 amu) were used to improve the mass accuracy.

Identification of the Peptic Digests of DmpFG. Using the unexchanged control sample, accurate masses of peptic digests of DmpFG were calculated on the basis of *m*/*z* data of ESI-Q-TOF spectra. The peptides were preliminarily identified on the basis of accurate masses by searching DmpFG sequence data with the ExPASy-FindPept tool (*36*). Typically, several possible peptides of DmpFG were indistinguishable since insufficient mass accuracy was obtained in the ESI-Q-TOF measurement, and therefore, peptide sequencing was carried out using a Waters CapLC system interfaced with an ESI-Q-TOF 2 mass spectrometer. Peptic digests of DmpFG (5 μL) were loaded onto a Symmetry 300 C18 trap column (0.35 mm × 5 mm), for desalting and concentration, followed by elution onto an Atlantis dC C18 NanoEase column (75 μm × 100 mm). Mobile phase A consisted of formic acid (0.1%) and acetonitrile (3%), while mobile phase B consisted of formic acid (0.1%) and acetonitrile (97%). The CapLC system was equilibrated with a mixture of 95% solvent A and 5% solvent B. The samples were loaded and desalted for 6 min in the trap column (20 μL/min) with the equilibration solvent. Then the flow was switched to the separating column, and a gradient from 5 to 50% mobile phase B was run (6 μL/min) over 50 min, followed by 5 min with 50% B, and then an increase to 95% B over 10 min. After the survey scan had been performed, MS/MS was performed online as peptides eluted from the column, selecting individual peptide precursors: the collision-

induced dissociation (CID) energy used for fragmentation was between 25 and 48 eV depending on the mass and charge state of the precursor ion. The peptides picked for MS/MS were mainly those with double and triple charges, and a few with quadruple and quintuple charges.

The raw data from MS/MS of peptic digests of DmpFG were first processed using MaxEnt3 and then loaded into the peptide sequencing program of the BioLynx module of MassLynx version 4.0. The sequence predictions were finally obtained by performing the automated MassSeq approach which often gave a partial sequence of the peptide. A combination of accurate mass and partial sequencing information resulted in the final assignments for peptic digests of DmpFG (*37*). The Q-TOF 2 instrument calibration was achieved via MS/MS of human [Glu^1]fibrinopeptide B (1569.6698 Da). The voltage on the capillary probe tip was set to 3.3 kV, and the voltage on the sample cone was 43 V.

Enzyme Kinetic Experiments. Acetaldehyde dehydrogenase activity was monitored by the reduction of NAD^+ at 340 nm in the presence of acetaldehyde and CoASH.

The apparent K_m values for NAD^+ and CoASH were estimated from initial rate measurement in 50 mM HEPES buffer (pH 8.0) containing 1 mM DTT at 25 °C. The reactions were started by addition of DmpFG protein (0.75 μg/mL) to the assay mixture containing substrates NAD^+, CoASH, and 38.4 mM acetaldehyde.

The examination of the effects of coenzyme A on DmpF was performed at pH 7, in 50 mM Na^+K^+ phosphate buffer at 25 °C. The DmpFG sample was buffer-exchanged with 50 mM Na^+K^+ phosphate buffer (pH 7), and TCEP-HCl was removed prior to further experiments. The assay mixtures contained 3.0 μg/mL DmpFG protein, 75.1 μM CoASH, 15.5 mM acetaldehyde, and various concentrations of NAD^+. To examine interactions of CoASH with DmpF, the following experiments were performed. The standard assay to which others were compared was initiated by addition of enzyme as the last component of the assay mixture. To test possible inhibition by CoASH, the enzyme was incubated with CoASH before addition of other components, and the reaction was initiated by addition of acetaldehyde. To examine whether NAD^+ could protect against inhibition by CoASH, the enzyme was incubated with NAD^+ prior to CoASH, and then the reaction was started by addition of acetaldehyde. The effects of DTT were tested using the same procedure as the CoASH inhibition assay except that the HEPES buffer already contained 1 mM DTT. Recovery of activity from the CoA-inhibited enzyme by the addition of DTT was examined using the same assay procedure that was used for CoASH inhibition except that 0.1 M DTT was added to the assay mixture after the incubation of enzyme with CoASH (final DTT concentration of 1 mM).

Automated Docking of CoASH to DmpF. The three-dimensional coordinates for the entire molecule of CoASH (coa_clean.pdb) were obtained from the HIC-Up Server (http://xray.bmc.uu.se/hicup). Atomic coordinates corresponding to the nucleotide portion of CoASH were initially superimposed onto those of the NAD^+ cofactor found in the DmpFG structure (PDB entry 1NVM) using LSQMAN (*38*). The atomic coordinates of CoASH corresponding to the pantetheine portion of the cofactor were manually adjusted by general bond torsions using O (*39*) such that all atoms resided within a cavity consisting of the DmpF active site and a tunnel connecting the active site to the protein surface. This model was selected as the candidate ligand for automated docking to DmpF using AUTODOCK (*40*). Eight of the 20 possible torsions in CoASH were active in the docking simulation. The grid of the docking simulation was defined by a 21 Å × 21 Å × 21 Å cube centered on the CoASH molecule within the DmpF active site. The docking simulation was performed using a Lamarckian genetic algorithm search routine with a population of 50 individuals and a maximum of 500000 energy evaluations. In total, 291 generations were analyzed. Molecular graphics were generated using PyMOL (*41*).

RESULTS

Hydrogen−Deuterium Exchange Experiments. To characterize the binding of NAD^+ and coenzyme A to DmpFG, hydrogen−deuterium exchange experiments were performed by mixing small volumes of DmpFG protein, DmpFG−NAD^+ complex, or DmpFG−CoASH complex with large volumes of D_2O-containing buffer. Cofactor binding sites would be expected to become inaccessible to D_2O as a result of shielding by any bound cofactors. Comparison of the mass spectra of peptides from pepsin digests of holo-DmpFG to those of apo-DmpFG following quenching at pH 2.5 and 0 °C allowed identification of sites where accessibility to solvent changed upon cofactor binding. In the NAD^+ or CoASH binding experiments, 2 mM NAD^+ or 2.3 mM CoASH permitted observation of reasonable MALDI MS signals. These concentrations also appeared to be saturating, since no significant increase in the number of amide hydrogens protected was observed with 4 mM NAD^+ or CoASH (data not shown). H−D exchange experiments were also performed with either NAD^+ (0.5 and 1 mM) or CoASH, and the same peptides exhibited amide hydrogen protection against H−D exchange, although the number of incorporated deuteriums increased (data not shown). Since the accessibility changes were the same at these different concentrations of cofactors, a single binding event was likely measured in these experiments.

To identify the pepsin-generated fragments of DmpFG obtained after quenching, we sequenced peptides using HPLC−ESI-Q-TOF MS/MS. A total of 86 peptides were observed, and 79 were identified (Figure 3). Seven peptides could not be characterized because of the weak signal and the interference from strong adjacent peaks. Among the 79 identified peptides, 42 were from DmpF, covering 89% of the sequence (Figure 3A), and 37 were from DmpG, covering 85% of the sequence (Figure 3B). Fewer identified peptides were observed in the MALDI-TOF spectra: 26 peptides from DmpF were observed, covering 69% of the sequence (Figure 3A), and 23 observed DmpG peptides accounted for 66% of the sequence of DmpG (Figure 3B). In the in- and back-exchange control experiments, 7−19% (12% average) of in-exchanges and 58−87% (67%) of back-exchanges were observed among the fragments showing amide hydrogen protection against H−D exchange.

From H−D exchange data, various numbers of amide hydrogens in peptides corresponding to DmpF residues 9−19, 36−63, 46−63, 155−174, 275−291, and 275−301 were found to be involved in protection against H−D exchange in the presence of a cofactor (Table 1). Incorpora-

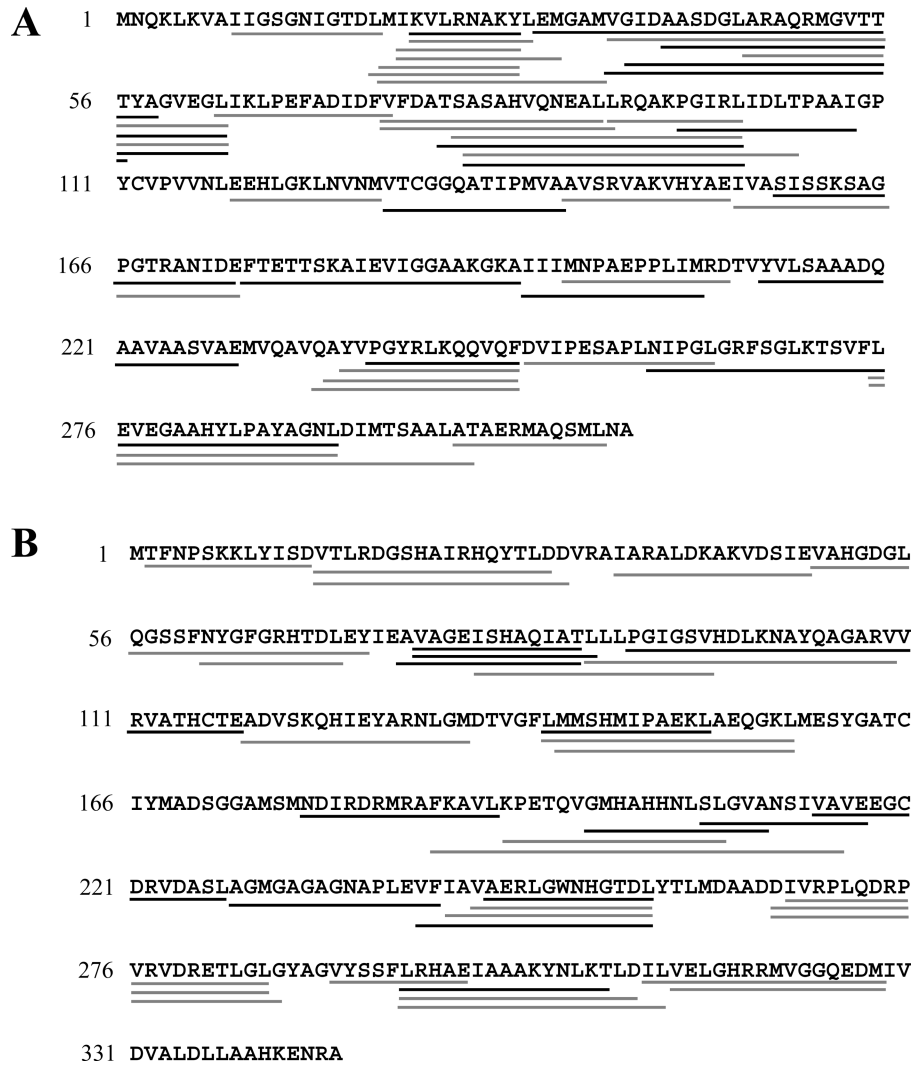

FIGURE 3: Identification of peptides from pepsin digests of DmpFG. (A) Peptides from DmpF identified using MS/MS are underlined and cover 89% of the sequence; fragments observed in the MALDI-TOF spectrum only are underlined in gray and cover 69% of the sequence. (B) Peptides from DmpG identified using MS/MS are underlined and cover 85% of the sequence; fragments observed in the MALDI-TOF spectrum only are underlined in gray and cover 66% of the sequence.

Table 1: H−D Exchange Parameters of Peptides of DmpF with Amide Hydrogen Protection upon Cofactor Binding[a]

peptic fragment of DmpF and corresponding mass ([M])	observed total no. of amide H atoms protected against H−D exchange binding at 15 min		no. of exchanged amide H atoms [rate constant (min^{-1})] for fast and slow phases[b]		
	NAD^+	CoASH	no cofactor	NAD^+	CoASH
residues 9−19 (1058.57)	3.2 ± 0.3	3.2 ± 0.2	4.1 ± 0.1 (10.6 ± 3.6) 2.3 ± 0.1 (0.3 ± 0.1)	1.7 ± 0.1 (7.4 ± 2.1) 1.5 ± 0.1 (0.4 ± 0.1)	1.5 ± 0.1 (7.2 ± 2.6) 1.8 ± 0.1 (0.4 ± 0.2)
residues 155−174 (1972.03)	3.1 ± 0.1	2.2 ± 0.1	9.7 ± 0.3 (9.0 ± 3.0) 4.4 ± 0.2 (0.4 ± 0.1)	8.3 ± 0.4 (7.6 ± 2.5) 2.7 ± 0.2 (0.4 ± 0.2)	9.0 ± 0.2 (7.6 ± 3.0) 3.1 ± 0.2 (0.4 ± 0.2)
residues 46−63 (1879.97)	3.0 ± 0.1	2.8 ± 0.2	−	−	−
residues 36−63 (2778.40)	4.2 ± 0.1	4.2 ± 0.2	12.6 ± 0.5 (6.1 ± 2.1) 5.9 ± 0.3 (0.3 ± 0.1)	8.8 ± 0.4 (5.7 ± 1.8) 5.4 ± 0.2 (0.3 ± 0.1)	9.0 ± 0.5 (5.7 ± 1.7) 5.4 ± 0.2 (0.3 ± 0.1)
residues 275−291 (1786.90)	1.2 ± 0.1	1.0 ± 0.1	−	−	−
residues 275−301 (2761.37)	4.1 ± 0.2	4.2 ± 0.2	7.8 ± 0.3 (5.5 ± 1.6) 7.8 ± 0.3 (0.4 ± 0.1)	4.5 ± 0.2 (4.3 ± 1.1) 6.9 ± 0.2 (0.3 ± 0.2)	4.4 ± 0.3 (4.3 ± 1.7) 7.2 ± 0.4 (0.3 ± 0.1)

[a] Data shown are averages for three independent experiments. [b] From fitting of deuterium exchange data to a double-exponential equation as shown in Figure 4 and as described in Experimental Procedures.

tion of a deuteron into these fragments was biphasic and almost reached the maximum after 10 min (Figure 4). Table 1 (columns 2 and 3) summarizes the total number of amide hydrogens protected at 15 min, determined directly from the mass shifts of the peptides at this time point. In addition, fitted deuterium incorporation rate constants and amplitudes from kinetics experiments such as those shown in Figure 4 are also given in Table 1 (columns 4−6). The limited number of data points that could be collected in the early time period means that the fitted rate constants for the faster reaction

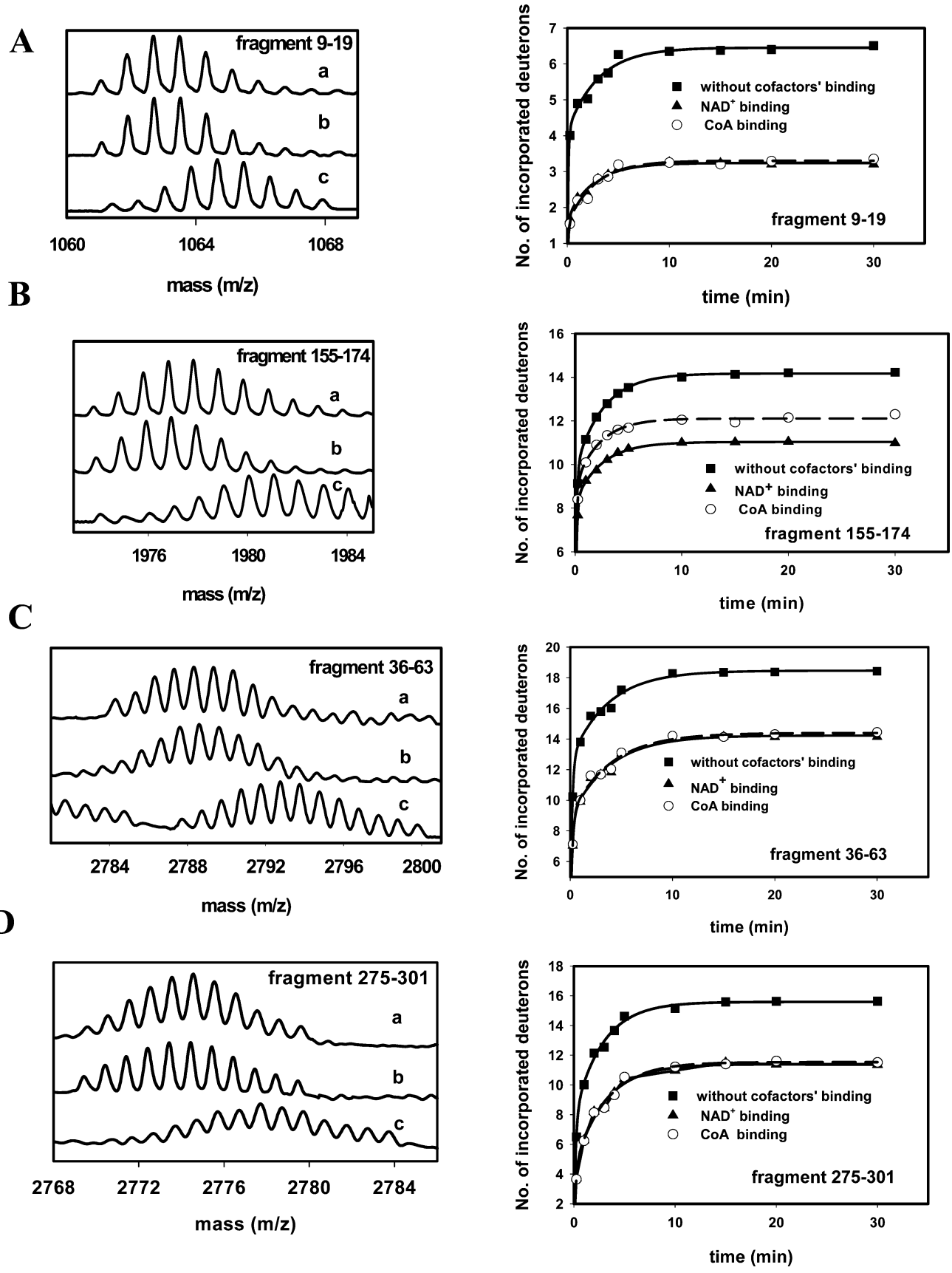

FIGURE 4: Isotopic envelopes of peptides at 10 min (left) and kinetics of incorporation of deuterium into DmpF-derived peptides (right). Each isotopic envelope indicates peptides from an enzyme that was (a) complexed with CoASH, (b) complexed with NAD^+, and (c) without cofactor binding. Kinetics plots are each fit to a double-exponential equation, as described in Experimental Procedures, with rate constants and amplitudes as in Table 1: (A) 1058.57 Da peptide (residues 9−19), (B) 1972.03 Da peptide (residues 155−174), (C) 2778.40 Da peptide (residues 36−63), and (D) 2761.37 Da peptide (residues 275−301).

Table 2: Effectiveness of NAD^+, CoASH, or NaCl in Eluting Native DmpFG Bound to an NAD^+ Affinity Column

apparent K_m for NAD^+ (μM)	apparent K_m for CoASH (μM)	eluted by NAD^+ (mM)	eluted by CoASH (mM)	eluted by NaCl (mM)
156	8.7	2	2.5	100

represent only a lower limit. Nevertheless, the rates and amplitudes of deuterium incorporation in the presence and absence of CoASH and NAD^+, as well as the difference in the total number of deuterons exchanged in the presence and absence of each cofactor, are useful probes of their binding sites.

The rates of hydrogen−deuterium exchange in the presence of CoASH, as well as the numbers of protons exchanged, were, with a few exceptions, indistinguishable from those observed with NAD^+, suggesting that the two cofactors share a single binding site. Furthermore, for all fragments, the number of protons exchanging in the slow phase was relatively constant regardless of the presence or absence of coenzyme, while the number exchanging in the fast phase was significantly decreased in the presence of either NAD^+ or CoASH. This implies that the more readily accessible backbone protons are blocked by cofactor binding, as one might expect.

Affinity Chromatography and Inhibition by CoASH. Several other experimental observations support the notion that CoASH and NAD^+ share a single cofactor binding site. Thus, either CoASH or NAD^+ was able to elute the enzyme from an NAD^+ affinity column (Table 2). Furthermore, preincubation of the enzyme with NAD^+ protected against inhibition by CoASH: inhibition was reversed by the addition of DTT, as one would expect if CoASH inhibition involves a covalent adduct with the enzyme via a disulfide bond at the active site (Figure 5). Since DmpF, like other CoASH-linked acetaldehyde dehydrogenases (*6, 10*), catalyzes a ping-pong reaction (our unpublished data) in which NAD^+ and acetaldehyde bind and NADH is released prior to CoASH binding, occupation of the same binding site by the two cofactors is feasible.

Comparison of H−D Exchange Results with the NAD^+−DmpF Crystal Structure. Patterns of protection against hydrogen−deuterium exchange in the presence of NAD^+ are consistent with the reported crystal structure of the DmpF−NAD^+ complex (*17*). This structure indicates that the peptide corresponding to DmpF residues 9−19 contains the dinucleotide-associated binding motif, GXGXXG (residues 11−16), involved in binding to the pyrophosphate, adenine, and ribose ring moieties of NAD^+ (*17*): in the presence of NAD^+, three amide hydrogens were protected against H−D exchange (Figure 4A, traces b and c and Table 1). The peptide corresponding to DmpF residues 155−174 includes a similar GXGXXA motif (residues 165−170) and mediates binding to pyrophosphate, the nicotinamide, and its ribose rings; for this peptide, three amide hydrogens were protected from H−D exchange upon NAD^+ binding (Figure 4B, traces b and c). Peptides corresponding to DmpF residues 36−63 (overlapping with residues 46−63) and 275−301 (overlapping with residues 275−291) are involved in binding to the adenine and nicotinamide rings, respectively: in the presence of NAD^+, four amide hydrogens were protected against deuterium replacement for each peptide (Figure 4C, traces b and c, and Figure 4D, traces b and c).

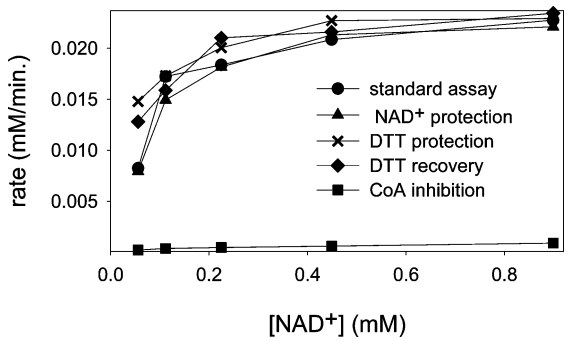

FIGURE 5: Inhibition by preincubation with CoASH and protection by NAD^+ and DTT. Assay conditions are described in Experimental Procedures.

Comparison of H−D Exchange Results with NAD^+ and CoASH. Very similar patterns of protection against H−D exchange were observed in the DmpF subunit upon CoASH binding. Thus, peptides corresponding to DmpF residues 9−19, 155−174, 36−63, 46−63, 275−291, and 275−301 all exhibited amide hydrogen protection against H−D exchange in the presence of either CoASH or NAD^+. Furthermore, in peptides corresponding to DmpF residues 9−19, 36−63, and 275−301, the same total number of hydrogens was protected against exchange as in NAD^+ binding (Figure 4A,C,D, traces a and c, respectively, and Table 1). However, only two amide hydrogens of the peptide corresponding to DmpF residues 155−174 were protected against deuterium replacement upon CoASH binding (Figure 4B, traces a and c). Significantly, no differences in H−D exchange upon cofactor binding were observed in the DmpG subunit (data not shown).

These results strongly suggest that the mode of CoASH binding to DmpF is very similar to that of NAD^+, reported for the X-ray structure. The nucleoside moiety of CoASH could interact with regions of peptides corresponding to DmpF residues 9−19, 155−174, and 36−63, all of which interact with the ADP moiety of NAD^+ (Figure 6). The segment of DmpF corresponding to residues 275−301 is likely to be associated with the binding of the pantetheine chain, which would need to approach Cys132 in the DmpF active site in preparation for nucleophilic attack on acetyl-S-Cys132, a postulated intermediate (*17*). Further insight into the interaction of CoASH with DmpF was obtained by modeling it using AUTODOCK.

Computer-Aided Modeling of the CoASH−DmpF Complex. Of the 50 conformers generated by AUTODOCK, 22 conformers organized into 14 clusters were obtained that exhibited energetically favorable binding to DmpF (energy of docking < -13 kcal/mol; rmsd compared to reference CoASH < 2.0 Å). One of the clusters (cluster 6) contained three CoASH conformers (6_1, 6_2, and 6_3) in which the thiol group is proximal to the thiol group of the DmpF Cys132 "B" conformation. The thiol group of conformer 6_1 was observed to be within 2.65 Å of the B thiol group of Cys132. The other two CoASH conformers within this cluster had thiol−thiol distances to the Cys132 B thiol of 2.79 and 3.65 Å, respectively. The 6_1 conformer was estimated by AUTODOCK to bind to DmpF with a ΔG of −11.3 kcal/mol and with a predicted dissociation constant of 5.04×10^{-9} M. Its rmsd compared to the input CoASH reference coordinates was calculated by AUTODOCK to be 1.64 Å.

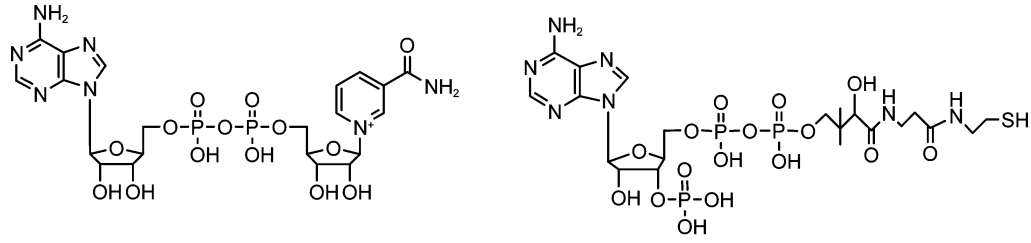

FIGURE 6: Comparison of NAD^+ and coenzyme A structures.

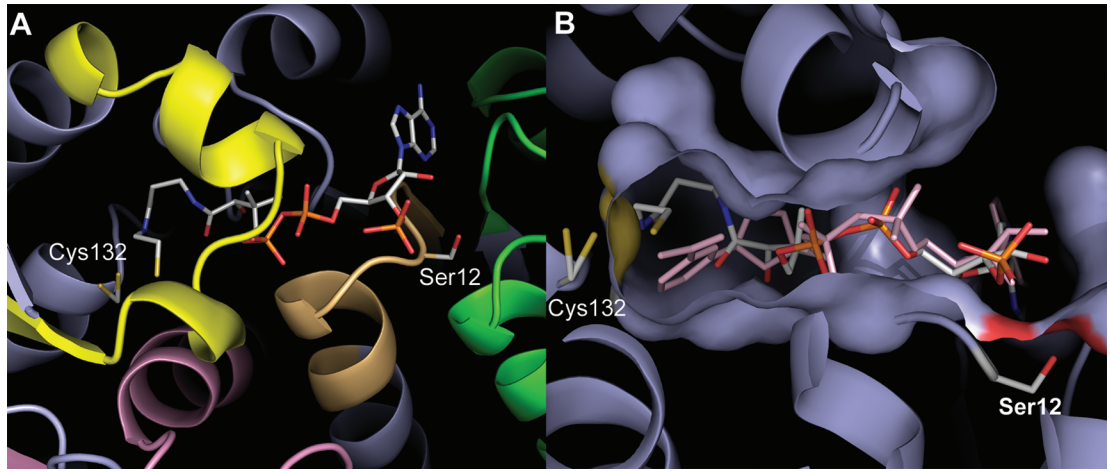

FIGURE 7: Models generated using AUTODOCK. (A) Binding of CoASH docked conformer 6_1 to DmpF. The CoASH cofactor is shown as sticks and colored according to element (blue for nitrogen, orange for phosphate, red for oxygen, white for carbon, and yellow for sulfur). The DmpF protein is shown in a cartoon representation (flat coils, helices). DmpF residues protected against H−D exchange are shaded as follows: residues 9−19, light orange; residues 36−63, green; residues 155−174, yellow; and residues 275−301, pink. The remaining DmpF residues are colored light blue. The two conformations of the Cys132 side chain are shown as sticks (white for carbon and yellow for sulfur). Residue Ser12, colored by elements, is also shown. (B) Superposition of CoASH conformer 6_1 with NAD^+ in the DmpF active site. A molecular surface, colored light blue, generated on DmpF shows the extent of the cavity containing the DmpF active site. The rest of the DmpF protein is shown in cartoon representation as in Figure 1A. Docked CoASH conformer 6_1 is shown as sticks (colored as in Figure 1A). The NAD^+ cofactor found in the crystal structure of the holoenzyme (PDB entry 1NVM) is shown as sticks and is colored light pink. These models were generated using PyMOL.

The binding of CoASH conformer 6_1 to DmpF is shown in Figure 7A. Extensive hydrogen bonding occurs between the pyrophosphate moiety of the 6_1 conformer and DmpF backbone amide groups. Two hydrogen bonds were observed between the 4′-phosphate of the docked CoASH and DmpF residue Ser12: one to the hydroxyl group of the side chain and one to the backbone carbonyl group of the residue. The 4′-phosphate is further stabilized by hydrogen bonding between its O4 atom and the backbone amide groups of Asn14 and Ile15.

Beyond the potential disulfide formation with CoASH at DmpF Cys132, hydrophilic interactions between the pantetheine moiety of CoASH conformer 6_1 and DmpF are not extensive. No hydrogen bonds are observed between the protein and the pantetheine carbonyl groups. A molecular surface projected onto DmpF indicates that the docked conformation of CoASH conformer 6_1 fully occupies the cavity containing the enzyme active site and superimposes with the NAD^+ cofactor observed in the X-ray crystal structure of the holoenzyme (Figure 7B).

DISCUSSION

Our hydrogen−deuterium exchange data establish that CoASH and NAD^+ share a cofactor binding site in the DmpF subunit of DmpFG. The changes in H−D exchange in the presence of the cofactor are consistent with the crystal structure of the enzyme−NAD^+ complex (*17*) and the model of the enzyme−CoASH complex derived here.

The observation that a single Rossmann fold can alternately bind nicotinamide cofactor and coenzyme A appears to be unique. $NAD(P)^+$-binding Rossmann folds have been characterized in many different dehydrogenases (*42*), and Rossmann folds that bind coenzyme A have also been characterized (*43*); however, to the best of our knowledge, a single Rossmann fold that binds both cofactors has not been described previously. Interestingly, the sequence of DmpF clusters in the Pfam database with the NAD^+-binding Rossmann fold of phosphorylating dehydrogenases such as aspartate semialdehyde dehydrogenase (*19*), rather than the CoASH-binding fold of succinyl-CoA synthetase (*43*). Furthermore, a three-dimensional structure-based search of the PDB archive using Secondary Structure Matching (SSM) (*44*) revealed the closest match to structures of glyceraldehyde-3-phosphate dehydrogenases, rather that CoA-binding Rossmann fold-based proteins (data not shown). Nevertheless, the NAD^+ and CoA-binding Rossmann folds are quite similar to one another (*42*).

Cofactor Binding Site Characterization. In DmpF, the observation that three amide hydrogens of the fragment of residues 9−19 were protected by NAD^+ against deuterium

replacement (Table 1) is in agreement with the crystal structure data. The AO3* oxygen atom of the adenine ribose of NAD^+ forms a hydrogen bond to the main chain nitrogen atom and the side chain hydroxyl oxygen atom of Ser12. The main chain nitrogens of Asn14 and Ile15 bind to the pyrophosphate through hydrogen bond interaction with AO2 and NO2 oxygen atoms, respectively. Meanwhile, the side chain of Ile15 and the nicotinamide ring of NAD^+ are involved in a van der Waals interaction.

Homologous interactions are observed in the modeled complex with CoASH. The O3* atom of the adenine ribose of CoASH H-bonds with the main chain nitrogen of Gly13 instead of that of Ser12 in the NAD^+−DmpF complex, while the main chain nitrogens of Asn14 and Ile15 hydrogen bond to O4 of CoASH. Furthermore, the side chain of Ile15 interacts with C12 of the pantetheine chain of CoASH, in place of the nicotinamide ring of NAD^+. The observation that three amide hydrogens in this region were protected against H−D exchange upon CoASH binding is thus consistent with the AUTODOCK model, although it should be noted that protection from H−D exchange need not necessarily correlate with the number of amide hydrogen bonds.

When NAD^+ and CoASH bind, three amide hydrogens and two amide hydrogens, respectively, of a peptide corresponding to DmpF residues 155−174 were protected from H−D exchange (Table 1). Two amide hydrogens may be protected by the hydrogen bonding interaction between the amide nitrogens of Gly165 and Gly167 and the pyrophosphate oxygen of NAD^+ (NO1 and AO1) (*17*) or CoASH (O5 and O1) in the modeled complex. The origin of the extra amide protected against exchange by NAD^+ may be the H-bonding interactions between the side chain nitrogen and carbonyl oxygen of Asn171 and NO3* and NO2* of the nicotinamide ribose. In the modeled CoASH complex, the side chain nitrogen and carbonyl oxygen of Asn171 appear to be involved in weaker van der Waals contacts with C6 and C7 of the pantetheine chain.

The labeling patterns of overlapping DmpF peptides corresponding to residues 46−63 and 36−63 indicate that within the shorter peptide (residues 46−63) three amide hydrogens are protected from H−D exchange while in the longer peptide one additional proton is protected (Table 1). While crystal structure data show that three residues, Val36, Gly37, and Ile38, within the DmpF sequence of residues 36−45 are involved in van der Waals interactions with NAD^+, no residue within the sequence of residues 46−63 is in direct contact with bound NAD^+. In this case, the observed protection against H−D exchange may result from protein conformational change that makes some amino acid residues less accessible and other residues more exposed to the solvent. In fact, a significant conformational change was observed upon cofactor binding to DmpFG in the crystal structure (*17*), as summarized in Figure 8A. The structural differences observed upon NAD^+ binding affect not only residues which directly interact with cofactor but also other regions which are located near the binding site or even farther from it (Figure 8B). Residues in positions 36−45 undergo a large movement upon NAD^+ binding, especially Asp39 and Ala40: these residues could not be matched with the corresponding residues in the apo structure. Residues 46−63 also shift considerably such that Thr54, Thr55, Thr56, and

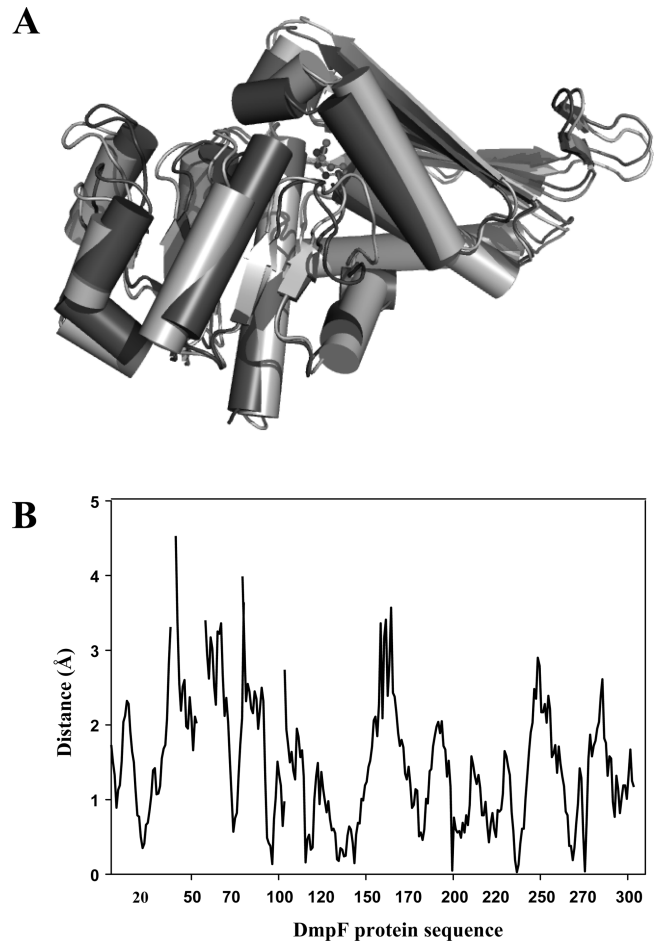

FIGURE 8: Comparison of DmpF (apo) and DmpF−NAD^+ (holo) structures based on PDB entry 1NVM. (A) Superimposition of holo-DmpF (chain H, dark gray) and apo-DmpF (chain F, light gray) backbones. Active site residue Cys132 is denoted by balls and sticks. (B) Cα distances of the aligned residues between holo- and apo-DmpF. The space gaps represent nonaligned residues. Three-dimensional structures of chains H (holo) and F (apo) of DmpF were aligned using SSM (http://www.ebi.ac.uk/msd-srv/ssm/cgi-bin/ssmserver). Cα distances of the corresponding residues were obtained for drawing the plot.

Tyr57 in the apo and holo structures do not overlap (Figure 8B). Thus, protection of the three amide hydrogens observed in the peptide corresponding to DmpF residues 46−63 is likely due to the conformational change caused by NAD^+ binding. Essentially identical H−D exchange behavior in peptides corresponding to DmpF residues 46−63 and 36−63 was observed upon CoASH binding (Table 1), in which three amide hydrogens were protected in the shorter peptide (residues 46−63) and one additional proton was protected in the longer peptide, suggesting that CoASH stimulates a conformational change in DmpF similar to that which occurs when NAD^+ binds.

Comparison of another pair of overlapping peptides, corresponding to DmpF residues 275−291 and 275−301, indicates that one and four amide hydrogens are protected upon NAD^+ binding, respectively (Table 1). In the DmpFG crystal structure, the side chain amide nitrogen of Asn290 contacts the carboxamide nitrogen of the bound NAD^+. One side chain carbon of Leu291 contacts the carboxamide oxygen of NAD^+, and the side chain CG and CE atoms of Met294 interact with NC5 and NC6 in the nicotinamide ring. In addition, alignment of the holo and apo structures indicates

that residues 285−294 undergo a large displacement upon NAD^+ binding (Figure 8B). We propose that protection of the four amide hydrogens in the peptide corresponding to residues 275−301 is due to the direct interaction of three residues, Asn290, Leu291, and Met 294, with the nicotinamide ring or to the conformational change associated with NAD^+ binding. The same H−D exchange events were observed in peptides corresponding to residues 275−291 and 275−301 upon CoASH binding as observed upon NAD^+ binding. The fact that no interaction occurred between residues 275−301 and CoASH in the model of the complex supports our hypothesis that protection of the four amide hydrogens is likely due to a conformational change similar to that observed upon NAD^+ binding.

In the crystal structure of DmpFG, Cys132 of DmpF is 3.4 Å from the nicotinamide ring of NAD^+. The covalent modification of an enzyme-based thiol group by CoASH, suggested by the results shown in Figure 5, could be explained by the close approach of the thiol group of bound CoASH to the thiol group of Cys132. In the CoASH−DmpF model, the 2.65 Å distance between the sulfur atom of Cys132 and the thiol group of CoASH is, given a reasonable degree of error in the model, potentially short enough for formation of a disulfide bond. Interestingly, the atoms at the end of the pantetheine chain, including atoms S1, C2, C3, N4, C5, and O5 of the carbonyl oxygen, are all proximal to atoms of Cys132, Thr131, or Val130 residues, which may help position the thiol group, allowing it to form the disulfide bond. Although formation of a disulfide bond appears to occur when CoASH is incubated with enzyme in the absence of other substrates, a close approach of the CoASH thiol would also be required for attack on a Cys132−thioacetyl intermediate in the proposed catalytic cycle (*17*).

Comparison with Other CoASH-Binding Proteins. More than 100 structures of CoASH-binding proteins in complex with the cofactor have been determined. The CoASH-binding folds for these proteins include a large variety of different topologies. Some folds are not exclusive to CoASH binding (the four-helix up-and-down bundle, the Rossmann fold, and the TIM barrel fold), while others have been reported in only CoASH-binding proteins to date (*45*). Only succinyl-CoA synthetase (*43, 46*), formyl-CoA transferase from *Oxalobacter formigenes* (*47*), and a protein of unknown function, Pfu-723267-001 from *Pyrococcus furiosus* (PDB entry 1Y81), have been shown to bind CoASH at a Rossmann fold, which appears to be the case with DmpF. However, none of these proteins has been reported to bind $NAD(P)^+$ also. The identification of structural features that allow the Rossmann fold of DmpF to bind either cofactor must await determination of the crystal structure of a complex with CoASH.

Conformations of the cofactors in the experimentally observed CoASH complexes of succinyl-CoA synthetase (SCS) and formyl-CoA transferase (FCT), and the NAD^+ complex of DmpF, are remarkably similar. The bound CoASH in succinyl-CoA synthetase and formyl-CoA transferase adopts an extended conformation. The distance between AC6 and PS1 is 17.3 Å in the CoASH of SCS, while it measures 16.5 Å in FCT: this is comparable with the 16.5 Å distance between AC6 and NC4 of NAD^+ bound in DmpF. The adenine rings of CoASH in both SCS and FCT, as well as the NAD^+ in DmpF, all are positioned in the anti conformation relative to the ribose group. The ribose ring of CoASH in SCS exhibits a 1′-exo conformation, not the more common 2′-endo conformation observed in CoASH of FCT and NAD^+ bound to DmpF, but the difference between the two conformations is not believed to be large (*46*). In the CoASH−SCS and NAD^+−DmpF complexes, the planes of the adenine ring and the axis connecting pyrophosphate are almost perpendicular to each other, whereas the adenine ring of CoASH in FCT and the axis are coplanar. These experimentally observed similarities support our observations that CoASH and NAD^+ share a binding site in DmpF.

Comparison to Other Proteins with Overlapping Ligand Binding Sites. Our finding that the two cofactors of DmpF share a binding site is an enzymatic property not without precedent in the literature, although reviews on this topic are scarce. Recently reported structures of enzymes with overlapping ligand binding sites include three reductases [methylenetetrahydrofolate reductase (*48, 49*), flavin reductase PheA2 (*50, 51*), and quinone reductase type 1 (*52, 53*)] and two other enzymes [chalcone synthase (*54*) and biosynthetic thiolase (*55*)].

These enzymes exhibit a diverse range of folds but share some common features. First, the substrates binding to the overlapping site often possess common structural elements; local conformational changes may also promote the recognition and binding of substrates. Second, these examples have in common ping-pong reaction mechanisms in which one of the substrates binds first and then a product is released to vacate the site for binding the next substrate. During catalysis, the formation of a covalently bound intermediate enzyme complex may be involved, e.g., a polyketide-S-Cys64 intermediate in chalcone synthase, acetyl-S-Cys89 intermediates in biosynthetic thiolase, and an acetyl-S-Cys132 intermediate in DmpF (our unpublished data). Third, in the examples cited, van der Waals forces dominate the interaction between the enzyme active site and substrates; limited numbers of H-bonds and the absence of electrostatic interactions lead to weak affinity, which favors the alternate binding and release of substrates and minimizes the strong interactions required for distinct recognition of structurally different substrates. These features are consistent with the data on DmpF that we report here.

As is apparently the case with DmpF, overlapping ligand binding sites are also associated with the Rossmann fold in a number of other enzymes. Malate dehydrogenase (decarboxylating) binds NAD^+, a substrate, and ATP, a regulator of catalytic activity, at a Rossmann fold with common binding interactions around their ADP moieties (*56–58*). Glyceraldehyde-3-phosphate dehydrogenase, the protein structurally most similar to DmpF, binds RNA and DNA competitively with NAD^+/NADH at a common site in the Rossmann fold (*59*). Furthermore, other dehydrogenases with Rossmann folds, such as alcohol dehydrogenase and lactate dehydrogenase, appear to bind RNA at the pyridine nucleotide cofactor binding site (*59*). The data presented here establish that DmpF is a member of a class of proteins that can bind multiple substrates at a single Rossmann fold. However, to the best of our knowledge, this is the only example thus far which binds NAD^+ and CoASH, two cofactors involved in the catalytic cycle of an enzyme.

ACKNOWLEDGMENT

We thank Alain Tessier and Bernard Gibbs for help and advice with the mass spectrometry experiments.

REFERENCES

1. Poels, P. A., Groen, B. W., and Duine, J. A. (1987) $NAD(P)^+$-independent aldehyde dehydrogenase from *Pseudomonas testosteroni*. A novel type of molybdenum-containing hydroxylase. *Eur. J. Biochem. 166*, 575–579.
2. Mukund, S., and Adams, M. W. (1993) Characterization of a novel tungsten-containing formaldehyde ferredoxin oxidoreductase from the hyperthermophilic archaeon, *Thermococcus litoralis*. A role for tungsten in peptide catabolism. *J. Biol. Chem. 268*, 13592–13600.
3. Perozich, J., Nicholas, H., Wang, B. C., Lindahl, R., and Hempel, J. (1999) Relationships within the aldehyde dehydrogenase extended family. *Protein Sci. 8*, 137–146.
4. Hempel, J., Nicholas, H., and Lindahl, R. (1993) Aldehyde dehydrogenases: Widespread structural and functional diversity within a shared framework. *Protein Sci. 2*, 1890–1900.
5. Sophos, N. A., and Vasiliou, V. (2003) Aldehyde dehydrogenase gene superfamily: The 2002 update. *Chem.-Biol. Interact.,* 143–144.
6. Rudolph, F. B., Purich, D. L., and Fromm, H. J. (1968) Coenzyme A-linked aldehyde dehydrogenase from *Escherichia coli*. I. Partial purification, properties, and kinetic studies of the enzyme. *J. Biol. Chem. 243*, 5539–5545.
7. Shone, C. C., and Fromm, H. J. (1981) Steady-state and pre-steady-state kinetics of coenzyme A linked aldehyde dehydrogenase from *Escherichia coli*. *Biochemistry 20*, 7494–7501.
8. Yan, R. T., and Chen, J. S. (1990) Coenzyme A-acylating aldehyde dehydrogenase from *Clostridium beijerinckii* NRRL B592. *Appl. Environ. Microbiol. 56*, 2591–2599.
9. Sohling, B., and Gottschalk, G. (1993) Purification and characterization of a coenzyme-A-dependent succinate-semialdehyde dehydrogenase from *Clostridium kluyveri*. *Eur. J. Biochem. 212*, 121–127.
10. Smith, L. T., and Kaplan, N. O. (1980) Purification, properties, and kinetic mechanism of coenzyme A-linked aldehyde dehydrogenase from *Clostridium kluyveri*. *Arch. Biochem. Biophys. 203*, 663–675.
11. Toth, J., Ismaiel, A. A., and Chen, J. S. (1999) The *ald* gene, encoding a coenzyme A-acylating aldehyde dehydrogenase, distinguishes *Clostridium beijerinckii* and two other solvent-producing clostridia from *Clostridium acetobutylicum*. *Appl. Environ. Microbiol. 65*, 4973–4980.
12. Sanchez, L. B. (1998) Aldehyde dehydrogenase (CoA-acetylating) and the mechanism of ethanol formation in the amitochondriate protist *Giardia lamblia*. *Arch. Biochem. Biophys. 354*, 57–64.
13. Palosaari, N. R., and Rogers, P. (1988) Purification and properties of the inducible coenzyme A-linked butyraldehyde dehydrogenase from *Clostridium acetobutylicum*. *J. Bacteriol. 170*, 2971–2976.
14. Buschhorn, H., Dürre, P., and Gottschalk, G. (1992) Purification and properties of the coenzyme A-linked acetaldehyde dehydrogenase of *Acetobacterium woodii*. *Arch. Microbiol. 158*, 132–138.
15. Stines-Chaumeil, C., Talfournier, F., and Branlant, G. (2006) Mechanistic characterization of the MSDH (methylmalonate semialdehyde dehydrogenase) from *Bacillus subtilis*. *Biochem. J. 395*, 107–115.
16. Powlowski, J., Sahlman, L., and Shingler, V. (1993) Purification and properties of the physically associated meta-cleavage pathway enzymes 4-hydroxy-2-ketovalerate aldolase and aldehyde dehydrogenase (acylating) from *Pseudomonas sp.* strain CF600. *J. Bacteriol. 175*, 377–385.
17. Manjasetty, B. A., Powlowski, J., and Vrielink, A. (2003) Crystal structure of a bifunctional aldolase-dehydrogenase: Sequestering a reactive and volatile intermediate. *Proc. Natl. Acad. Sci. U.S.A. 100*, 6992–6997.
18. Finn, R. D., Mistry, J., Schuster-Bockler, B., Griffiths-Jones, S., Hollich, V., Lassmann, T., Moxon, S., Marshall, M., Khanna, A., Durbin, R., Eddy, S. R., Sonnhammer, E. L., and Bateman, A. (2006) Pfam: Clans, web tools and services. *Nucleic Acids Res. 34*, D247–D251.
19. Hadfield, A., Shammas, C., Kryger, G., Ringe, D., Petsko, G. A., Ouyang, J., and Viola, R. E. (2001) Active site analysis of the potential antimicrobial target aspartate semialdehyde dehydrogenase. *Biochemistry 40*, 14475–14483.
20. Dubourg, H., Stines-Chaumeil, C., Didierjean, C., Talfournier, F., Rahuel-Clermont, S., Branlant, G., and Aubry, A. (2004) Expression, purification, crystallization and preliminary X-ray diffraction data of methylmalonate-semialdehyde dehydrogenase from *Bacillus subtilis*. *Acta Crystallogr. D60*, 1435–1437.
21. Liu, Z. J., Sun, Y. J., Rose, J., Chung, Y. J., Hsiao, C. D., Chang, W. R., Kuo, I., Perozich, J., Lindahl, R., Hempel, J., and Wang, B. C. (1997) The first structure of an aldehyde dehydrogenase reveals novel interactions between NAD and the Rossmann fold. *Nat. Struct. Biol. 4*, 317–326.
22. Cobessi, D., Tete-Favier, F., Marchal, S., Branlant, G., and Aubry, A. (2000) Structural and biochemical investigations of the catalytic mechanism of an NADP-dependent aldehyde dehydrogenase from *Streptococcus mutans*. *J. Mol. Biol. 300*, 141–152.
23. Weiner, H., and Hurley, T. D. (2005)NADP22 Binding to Dehydrogenases. In *Encyclopedia of Life Sciences*, John Wiley & Sons, Ltd., Chichester, U.K.
24. Skarzynski, T., Moody, P. C., and Wonacott, A. J. (1987) Structure of holo-glyceraldehyde-3-phosphate dehydrogenase from *Bacillus stearothermophilus* at 1.8 Å resolution. *J. Mol. Biol. 193*, 171–187.
25. Al-Karadaghi, S., Cedergren-Zeppezauer, E. S., and Hovmoller, S. (1994) Refined crystal structure of liver alcohol dehydrogenase-NADH complex at 1.8 Å resolution. *Acta Crystallogr. D50*, 793–807.
26. Miroux, B., and Walker, J. E. (1996) Over-production of proteins in *Escherichia coli*: Mutant hosts that allow synthesis of some membrane proteins and globular proteins at high levels. *J. Mol. Biol. 260*, 289–298.
27. Sambrook, J., Fritsch, E. F., and Maniatis, T. (1989) *Molecular Cloning: A Laboratory Manual*, 2nd ed., Cold Spring Harbor Laboratory Press, Plainview, NY.
28. Shingler, V., Powlowski, J., and Marklund, U. (1992) Nucleotide sequence and functional analysis of the complete phenol/3,4-dimethylphenol catabolic pathway of *Pseudomonas* sp. strain CF60. *J. Bacteriol. 174*, 711–724.
29. Tabor, S., and Richardson, C. C. (1985) A bacteriophage T7 RNA polymerase/promoter system for controlled exclusive expression of specific genes. *Proc. Natl. Acad. Sci. U.S.A. 82*, 1074–1078.
30. Tynan, J., Forde, J., McMahon, M., and Mulcahy, P. (2000) Synthesis of a highly substituted N^6-linked immobilized NAD^+ derivative using a rapid solid-phase modular approach: Suitability for use with the kinetic locking-on tactic for bioaffinity purification of NAD^+-dependent dehydrogenases. *Protein Expression Purif. 20*, 421–434.
31. Mandell, J. G., Falick, A. M., and Komives, E. A. (1998) Measurement of amide hydrogen exchange by MALDI-TOF mass spectrometry. *Anal. Chem. 70*, 3987–3995.
32. Mandell, J. G., Baerga-Ortiz, A., Akashi, S., Takio, K., and Komives, E. A. (2001) Solvent accessibility of the thrombin-thrombomodulin interface. *J. Mol. Biol. 306*, 575–589.
33. Andersen, M. D., Shaffer, J., Jennings, P. A., and Adams, J. A. (2001) Structural characterization of protein kinase A as a function of nucleotide binding. Hydrogen-deuterium exchange studies using matrix-assisted laser desorption ionization-time of flight mass spectrometry detection. *J. Biol. Chem. 276*, 14204–14211.
34. Pentz, L., and Thornton, E. R. (1967) Isotope effects on the basicity of 2-nitrophenoxide, 2,4-dinitrophenoxide, hydroxide, and imidazole in protium oxide-deuterium oxide mixtures. *J. Am. Chem. Soc. 89*, 6931–6938.
35. Resing, K. A., and Ahn, N. G. (1998) Deuterium exchange mass spectrometry as a probe of protein kinase activation. Analysis of wild-type and constitutively active mutants of MAP kinase kinase-1. *Biochemistry 37*, 463–475.
36. Gattiker, A., Bienvenut, W. V., Bairoch, A., and Gasteiger, E. (2002) FindPept, a tool to identify unmatched masses in peptide mass fingerprinting protein identification. *Proteomics 2*, 1435–1444.
37. Mann, M., and Wilm, M. (1994) Error-tolerant identification of peptides in sequence databases by peptide sequence tags. *Anal. Chem. 66*, 4390–4399.
38. Kleywegt, G. J., and Jones, T. A. (1994) A super position. *CCP4/ESF-EACBM Newsletter on Protein Crystallography 31*, 9–14.
39. Jones, T. A., Zou, J. Y., Cowan, S. W., and Kjeldgaard, M. (1991) Improved methods for building protein models in electron density maps and the location of errors in these models. *Acta Crystallogr. A47*, 110–119.

40. Morris, G. M., Goodsell, D. S., Halliday, R. S., Huey, R., Hart, W. E., Belew, R. K., and Olson, A. J. (1998) Automated docking using a Lamarckian genetic algorithm and an empirical binding free energy function. *J. Comput. Chem. 19*, 1639–1662.
41. DeLano, W. L. (2002) *The PyMOL Molecular Graphics System*, DeLano Scientific, San Carlos, CA.
42. Bashton, M., and Chothia, C. (2002) The geometry of domain combination in proteins. *J. Mol. Biol. 315*, 927–939.
43. Wolodko, W. T., Fraser, M. E., James, M. N., and Bridger, W. A. (1994) The crystal structure of succinyl-CoA synthetase from *Escherichia coli* at 2.5-Å resolution. *J. Biol. Chem. 269*, 10883–10890.
44. Krissinel, E., and Henrick, K. (2004) Secondary-structure matching (SSM), a new tool for fast protein structure alignment in three dimensions. *Acta Crystallogr. D60*, 2256–2268.
45. Engel, C., and Wierenga, R. (1996) The diverse world of coenzyme A binding proteins. *Curr. Opin. Struct. Biol. 6*, 790–797.
46. Fraser, M. E., James, M. N., Bridger, W. A., and Wolodko, W. T. (1999) A detailed structural description of *Escherichia coli* succinyl-CoA synthetase. *J. Mol. Biol. 285*, 1633–1653.
47. Ricagno, S., Jonsson, S., Richards, N., and Lindqvist, Y. (2003) Formyl-CoA transferase encloses the CoA binding site at the interface of an interlocked dimer. *EMBO J. 22*, 3210–3219.
48. Pejchal, R., Sargeant, R., and Ludwig, M. L. (2005) Structures of NADH and CH_3-H_4folate complexes of *Escherichia coli* methylenetetrahydrofolate reductase reveal a spartan strategy for a ping-pong reaction. *Biochemistry 44*, 11447–11457.
49. Trimmer, E. E., Ballou, D. P., and Matthews, R. G. (2001) Methylenetetrahydrofolate reductase from *Escherichia coli*: Elucidation of the kinetic mechanism by steady-state and rapid-reaction studies. *Biochemistry 40*, 6205–6215.
50. van den Heuvel, R. H., Westphal, A. H., Heck, A. J., Walsh, M. A., Rovida, S., van Berkel, W. J., and Mattevi, A. (2004) Structural studies on flavin reductase PheA2 reveal binding of NAD^+ in an unusual folded conformation and support novel mechanism of action. *J. Biol. Chem. 279*, 12860–12867.
51. Kirchner, U., Westphal, A. H., Muller, R., and van Berkel, W. J. (2003) Phenol hydroxylase from *Bacillus thermoglucosidasius* A7, a two-protein component monooxygenase with a dual role for FAD. *J. Biol. Chem. 278*, 47545–47553.
52. Faig, M., Bianchet, M. A., Talalay, P., Chen, S., Winski, S., Ross, D., and Amzel, L. M. (2000) Structures of recombinant human and mouse NAD(P)H:quinone oxidoreductases: Species comparison and structural changes with substrate binding and release. *Proc. Natl. Acad. Sci. U.S.A. 97*, 3177–3182.
53. Li, R., Bianchet, M. A., Talalay, P., and Amzel, L. M. (1995) The three-dimensional structure of NAD(P)H:quinone reductase, a flavoprotein involved in cancer chemoprotection and chemotherapy: Mechanism of the two-electron reduction. *Proc. Natl. Acad. Sci. U.S.A. 92*, 8846–8850.
54. Ferrer, J. L., Jez, J. M., Bowman, M. E., Dixon, R. A., and Noel, J. P. (1999) Structure of chalcone synthase and the molecular basis of plant polyketide biosynthesis. *Nat. Struct. Biol. 6*, 775–784.
55. Modis, Y., and Wierenga, R. K. (2000) Crystallographic analysis of the reaction pathway of *Zoogloea ramigera* biosynthetic thiolase. *J. Mol. Biol. 297*, 1171–1182.
56. Hsu, W. C., Hung, H. C., Tong, L., and Chang, G. G. (2004) Dual functional roles of ATP in the human mitochondrial malic enzyme. *Biochemistry 43*, 7382–7390.
57. Yang, Z., Lanks, C. W., and Tong, L. (2002) Molecular mechanism for the regulation of human mitochondrial $NAD(P)^+$-dependent malic enzyme by ATP and fumarate. *Structure 10*, 951–960.
58. Yang, Z., Floyd, D. L., Loeber, G., and Tong, L. (2000) Structure of a closed form of human malic enzyme and implications for catalytic mechanism. *Nat. Struct. Biol. 7*, 251–257.
59. Nagy, E., Henics, T., Eckert, M., Miseta, A., Lightowlers, R. N., and Kellermayer, M. (2000) Identification of the NAD^+-binding fold of glyceraldehyde-3-phosphate dehydrogenase as a novel RNA-binding domain. *Biochem. Biophys. Res. Commun. 275*, 253–260.

BI800349K